Lasers in Manufacturing Conference 2021

Cut edge quality in laser ablation of micrometer-scale grating structures

Meike Zilm[a,*], Tim Radel[a]

[a]*BIAS - Bremer Institut für angewandte Strahltechnik GmbH, Klagenfurter Str. 5, 28359 Bremen, Germany*

Abstract

During the production of grid structures heat accumulation occurs due to the limited surface area for heat dissipation via the ridge structures. This impairs the edge quality, affecting the ridge width and rectangularity. Due to thermal stresses and expansions, in combination with the low stiffness of the ridges, distortion or failure of these can occur. The aim of this study is to quantify the influence of the strategy for cutting out a single cutout with regard to the cut edge quality. For this purpose, 100 µm thick aluminum foils are processed by means of picosecond laser with different scanning strategies and subsequently examined for their ridge width. It is shown that both the global and local scanning strategy must be taken into account. Thereby, the standard deviation of the ridge width can mainly be reduced by a suitable global strategy. Imperfections at the ridges i.e. necking at the account points, local thickening and ridge deformation can be reduced or even prevented by the local scanning strategy.

Keywords: micro cutting; aluminum foils; microstructure

1. Introduction

The cutting of metallic foils and parts by lasers has established as a tool for various industrial applications. Remote laser cutting is used, for example, in aerospace (Qin 2015), medical devices (Baumann et al. 2019), or batteries in the automotive industry (Pfleging 2018). Pfleging (2018) showed that remote laser cutting of electrodes for batteries was one of the first laser technologies to be successfully transferred to industrial high-energy battery production. According to Baumann et al. (2019) the cutting quality is of very high importance in this application, as cut edge defects can, for example, pierce insulators and thus lead to a short circuit. Tóth

*Meike Zilm. Tel.: +49 421 218-58045; fax: +49 421 218-58063 .
E-mail address: zilm@bias.de .

et al. (2011) shows another field of application in the field of electro-optical lenses for focusing electron beams in electron spectroscopy. For this purpose, grid structures in the micrometer range are produced by laser processing and deep-drawn in a second production step.

During remote laser cutting with pulsed laser sources, the irradiated material evaporates. This leads to the formation of a vapor cavity as a result of which the kerf is formed. Schulz et al. (2013) showed that shorter pulse durations in the pico- or femtosecond range are necessary to introduce only a small amount of heat into the material. By using ultra-short pulsed lasers with wavelengths adapted to the material, the quality of the ablation process can be significantly increased compared to long pulses. Cut quality studies by Leone et al. (2016) showed that in a nitrogen environment at a pressure of 10 bar, the surface quality depends mainly on the scanning speed. In addition, surface finish studies by Gillner (2015) showed that surface roughness can be reduced to Ra < 0.7 µm by optimizing the energy input. Mangang et al. (2016) showed that the aspect ratio of the kerf can be increased by using shorter pulse durations. According to Park (2021), this can also be increased by increasing the number of passes at low fluence.

Czotscher et al. (2016a) proves that during the fabrication of the grid structures for electro-optical lenses, there is heat build-up due to the limited surface area for heat dissipation via the ridge structures, resulting in reduced cut edge qualities. The quality of the cut edge is an important parameter for a high imaging quality and so that high true strains can be achieved. Characteristics that define the quality of the cut edge and grid structure are e.g., the burr formation, the ridge width, the ridge width deviation and the squareness of the grid. Simons et al. pointed out defects that can occur during the fabrication of grids by laser ablation. There include not cut out slugs, burr formation, distortion, cracking or melting of the ridges due to thermal stresses and expansions in combination with a low stiffness of these. Figure 1 shows some of the defects that are possible in the manufacture of grids.

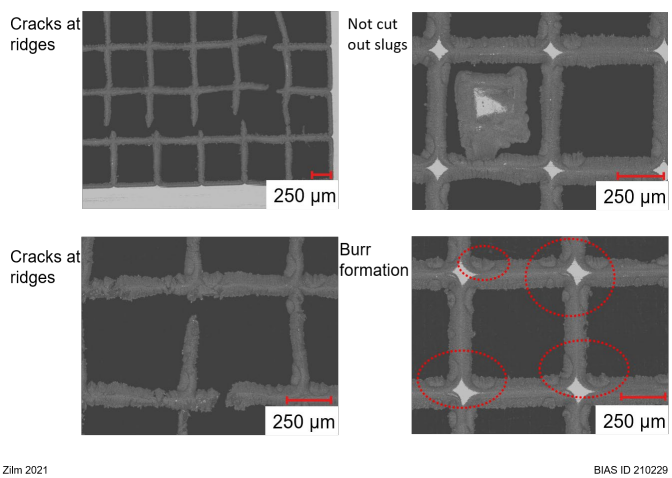

Fig. 1. Possible defects in grids

Further investigations by Czotscher et al. (2016b) in the processing of grids in the micro range showed that a low pulse overlap positively affects the ridge width deviation. Further investigations by Simons et al. (2020) showed that even an adapted scan strategy for laser processing of grids can reduce the ridge width deviation to less than 8 µm. Here, cutouts were machined that were more than one cutout width away from the last machined cutout. Czotscher (2017) also showed that a reduction of the ridge width deviation could also be observed by a scanning strategy in which the cutouts are machined helically from the inside to the outside.

In the state of the research, the influence of various laser parameters such as scanning speed, pulse duration, ambient pressure, and scanning strategy could be shown. Previous research mainly focused on the global scanning strategy of the grid structures rather than the individual cutouts. The influence of the laser start/end point and their influence on failure mechanisms of the ridge structures have not been analyzed. Gladush (2011) provided an approach for this. They showed that the melt surface temperature at the end of the pulse exceeded the melting temperature by one and a half times. This caused the melt boundary to move forward after the laser was turned off. This heat input could promote ridge cracking.

One approach to distribute the heat in the part in a more targeted way to improve the quality of the cut edges and the ridges is an adapted scan strategy of the individual cutouts and an optimization of the sequence for cutting out the cutouts. When cutting out a single cutout, a lot of heat energy can be dissipated via the slug that falls out. For this reason, the scanning strategy consists of several cuts, so that the slug is cut out in the first step and the geometry is completed in the following steps. In this work, different laser scanning strategies for cutting out the individual cutouts, as well as the entire grid, are analyzed with regard to the cut edge quality. In addition, the influence of the laser starting point and end point of the bar structures are investigated. In this study, a picosecond laser is used to fabricate the microstructures.

2. Experimental setup and procedure

2.1. Materials and setup for pulsed remote laser cutting

A picosecond laser from Trumpf (TruMicro 5050) was used to produce the grid structures in the micro range. The laser emits at a wavelength of 1030 nm and a pulse duration < 10 ps. The scanner used is the hurry SCAN II scanner system from SCANLAB with an aperture of 14 mm and a focal length of 160 mm. The laser has a laser beam diameter of 45 µm at the focus and achieves an average power of 50 W at a frequency of 200 kHz. Pulse energy between 25 mJ and 112.5 mJ was used to machine the grids at scan speeds between 200 mm/s and 450 mm/s.

In this study, the focal plane of the laser beam was placed on the surface of the metal foils, and the relative motion for patterning was performed directly through the scanner. This experimental setup, shown in Figure 2, was used to machine aluminum foils (EN AW-1050 material condition H111, i.e. Al99.5) with a foil thickness of d = 100 µm. The metal foils were clamped in a holder for machining so that they were uniformly stretched without wrinkles. Increased clamping of the foils allowed the cutout slugs to fall out. To protect the aluminum foils from oxidation during the machining process, the machining area was flooded with argon.

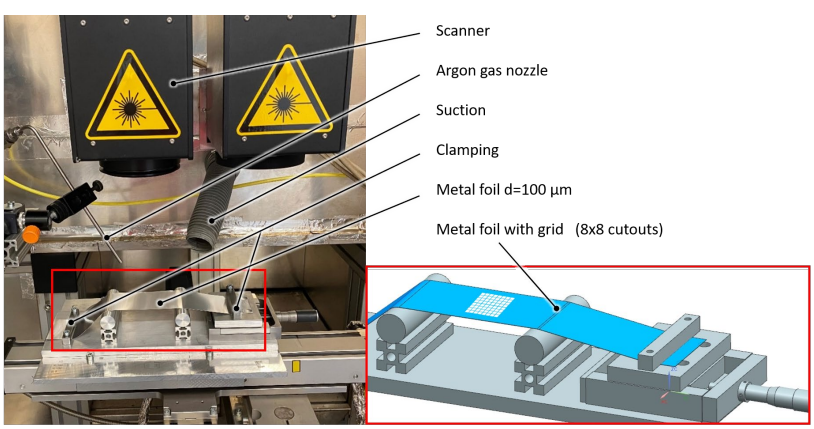

Fig. 2. Experimental setup for pulsed remote laser cutting of grids

2.2. Scanning strategies for grid and slug

For grating structuring, the scanning strategy is divided into local and global scanning strategy. The local scan strategy describes the strategy for cutting out a single cutout. The global scan strategy describes the strategy in which order the cutouts of the whole grid are structured one after the other. The different local, as well as global scan strategies are shown in Figure 3.

The local scan strategy of the cutouts consists of three different parameters, which work from the inside to the outside until the desired final geometry is reached. Here, the first parameter (Fig. 3 red) is used to cut out the slug. In addition, heat can be dissipated by the slug falling out. The innermost parameter consists of four vectors that overlap slightly to safely separate the slug. The outer two parameters (Fig. 3 green and blue) are used to smooth the edges and to finalize the final geometry. Table 1 shows the laser parameters used for the three scan vectors (red, green, blue). To determine the influence of the laser start and end point, these are varied for the outer two parameters. The start points were placed in the corner of the rectangles, inside the cutout and they were placed at half of the cutout length.

The global scan strategy describes the order in which the individual cutouts are processed one after the other. A distinction is made between two strategies. In the first, the cutouts are processed line by line, and in the second, the cutouts are processed from the inside to the outside with the maximum possible distance between them. The global and local scan strategies are combined with each other.

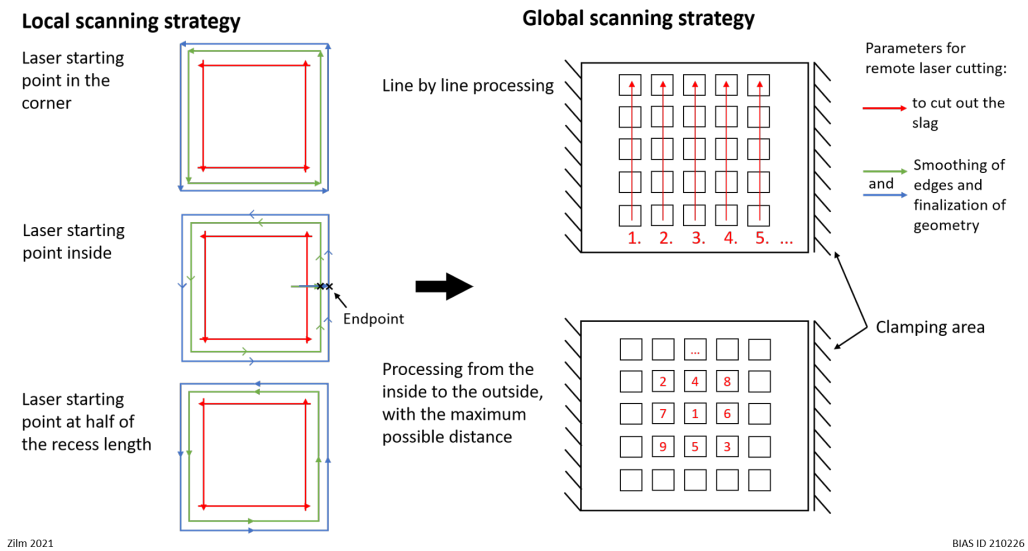

Fig. 3. Visualization of the analysed local and global scanning strategies

Table 1. Laser parameters

Color of the scan vector	Frequency [kHz]	Scanning speed [mm/s]	Pulse energy [µJ]	Repetitions [n]
red	200	200	112.5	40
green	200	250	50	30
blue	200	450	25	20

In addition, the six different scanning strategies were combined with different transmission levels. The transmission T of a grid structure is defined by the ratio of the cutouts to the total area. It is calculated from the ridge width b and the edge length of the cutout L (see equation 1, Figure 4). The length L of the cutout is composed of the scan length a and the ablation width c of the three scan paths (Figure 4). In order for the resulting cutouts to reach a size of 500 µm x 500 µm, an ablation width of all three parameters was determined. In single track tests, an ablation width of 45 µm was determined (Figure 4). Here, the section that is ablated from the red scan path inside is subtracted from this. The ablation width is thus measured from the center of the first scan path (red) to the edge of the ridge. Due to this ablation width of 45 µm, the innermost red scan paths have a length of 410 µm. The transmission is differentiated between the nominally set transmission (equation 1) and the resulting transmission. The transmission of the grid is varied between 70 % and 80 %. To vary the transmission of the grating, the ridge width is varied. Narrower ridge widths lead to higher transmission values. The resulting ridge widths are between 60 µm and 100 µm. This is constant for all experiments. The nominal size of the cutouts in these experiments is 500 µm x 500 µm.

$$T = \frac{L^2}{(L+b)^2}, \quad L = a + c \tag{1}$$

Grids with 8 x 8 cutouts were produced using these scanning strategies and transmissions.

2.3. Measuring the ridge width

To measure the ridge width, microscope images were first taken from the top surface using a 3D laser confocal microscope (model VK-9710). The ridge width was measured with a confocal microscope. The ridges have a trapezoidal shape in cross-section, so the ridge width was measured at the widest point. From the captured microscope images, the ridge widths were measured at three locations on the ridges and averaged. The ridge width deviation (standard deviation) of a ridge is calculated from these ridge widths, and the ridge width deviation of the entire grid is determined from this. Figure 4 shows the original image of the microscope of a grid. The ridge width in horizontal and vertical direction was then determined.

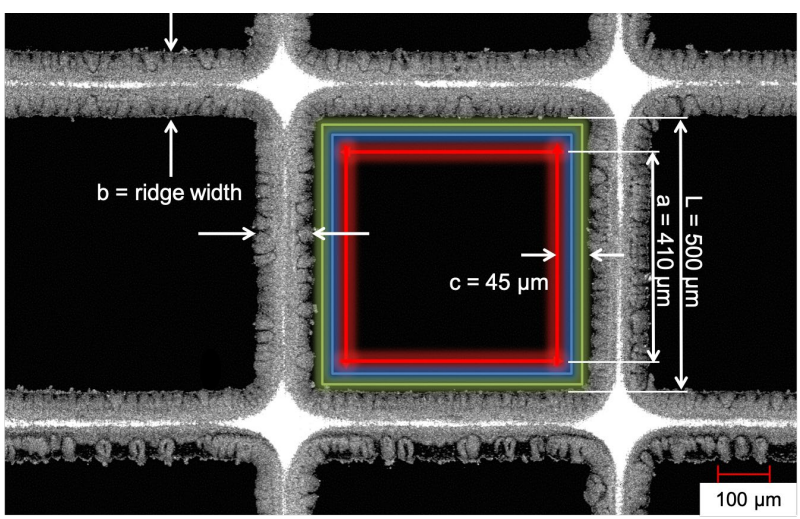

Zilm 2021 BIAS ID 210227

Fig. 4. Measuring of the ridge width

3. Results

Figure 5 shows the influence of the local and global strategies on the ridge width and Figure 6 shows the corresponding standard deviations.

Figure 5 shows that the global scanning strategies "line by line" generally leads to higher resulting ridge widths compared to the nominal ridge width. Furthermore, it can be seen from the figure that the local scanning strategies "at half of te recess length" leads to the smallest ridge widths, followed by the strategies "inside" and "in the corner". The scanning strategy "line by line" in combination with the local scanning strategy "at half of the recess length" leads to ridge widths that are smaller than the nominal ridge width.

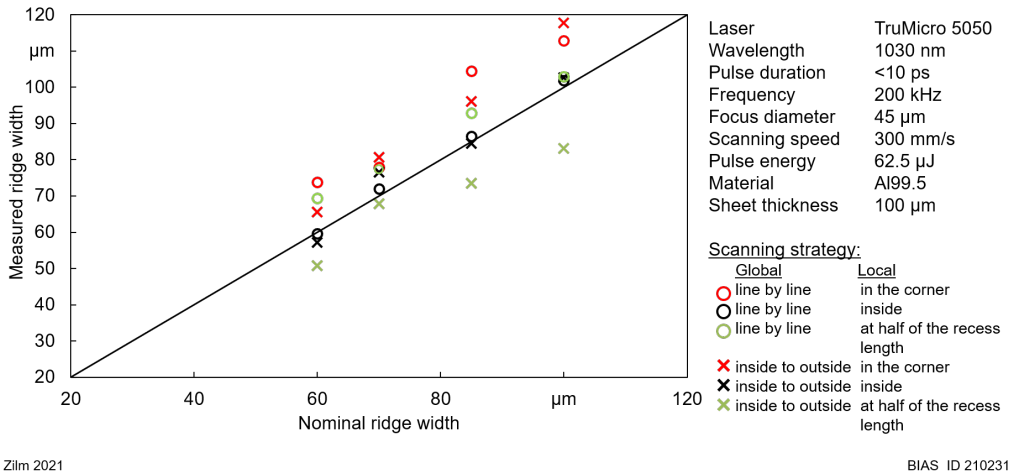

Fig. 5. Influence of the global and local scanning strategies on the ridge width

The global scanning strategy "inside to outside" leads to smaller standard deviations overall (Figure 6). Figure 6 shows that the local scanning strategies "at half of the recess length" and "in the corner" lead to significantly higher standard deviations, than the local scanning strategy "inside". The lowest standard deviations are achieved with the global scanning strategy "inside to outside" in combination with the local scanning strategy "inside". On average, this results in a standard deviation of 2.85 µm. The results show that for all nominal ridge widths the standard deviation is reduced by the scanning strategies "inside to outside". On average, the standard deviation was reduced from 3.8 µm to 3.0 µm. An increase in the standard deviation with decreasing ridge widths can be seen with both scanning strategies.

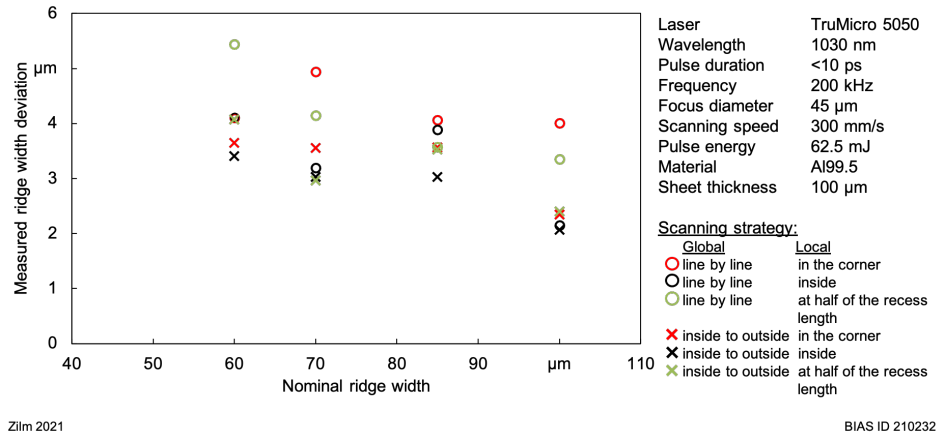

Fig. 6. Influence of the global and local scanning strategies on the standard deviation

Figure 7 shows the density function of the ridge widths at 80 % nominal transmission. The ridge width distributions of all scanning strategies are normally distributed. The statistical distribution of the ridge widths demonstrates clearly that the local scanning strategy "inside" can narrow the function, so that the probability for ridge widths around the mean value are significantly higher. As a result, the probability of ridge widths that are too narrow and could lead to failure is significantly lower.

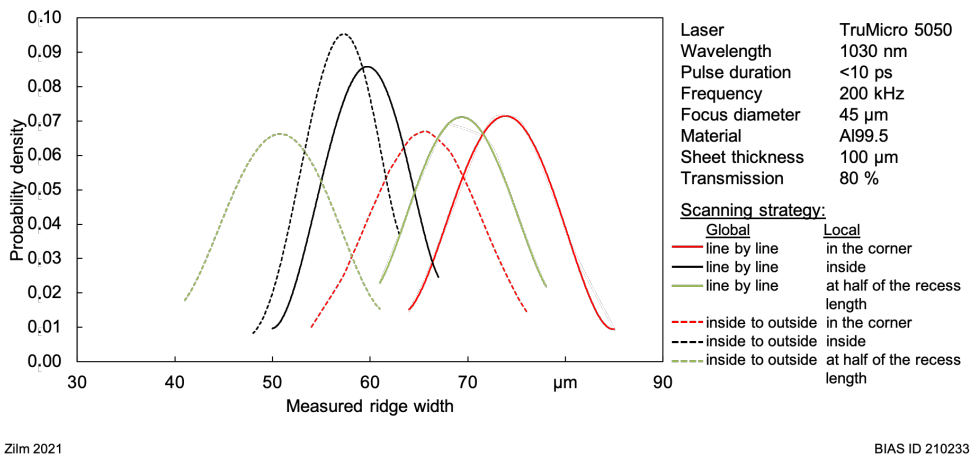

Fig. 7. Ridge width distribution at 80 % nominal transmission

The determined transmittances of the grids are shown in Figure 8. It is shown that the local scanning strategies "in the corner" do not achieve the nominal transmission. With the other strategies, the nominal transmission could be achieved. Only the scanning strategy "line by line" in combination with the local scanning strategy "at half of the recess length" leads to a too high measured transmission.

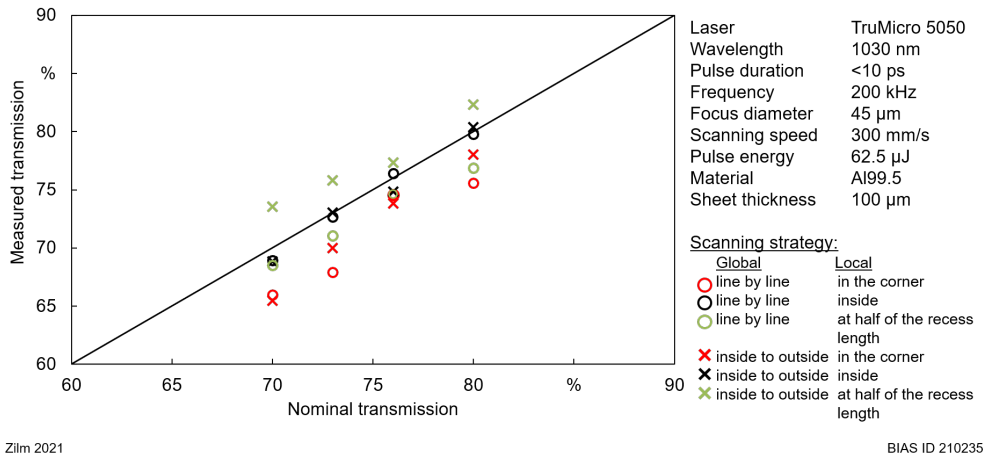

Fig. 8. Influence of the global and local scanning strategies on the transmission

To further investigate the influence of local scanning strategies and laser start and end points, the following Figure 9 shows detailed microscope images of the ridges with different kinds of imperfections. With the local scanning strategies "in the corner" there is a necking at the account points. The gratings made with the local scanning strategies "inside" show a thickening at some ridges, at the laser end point. The local scanning strategies "at half of the recess length" leads to a deformation especially at the horizontal ridges.

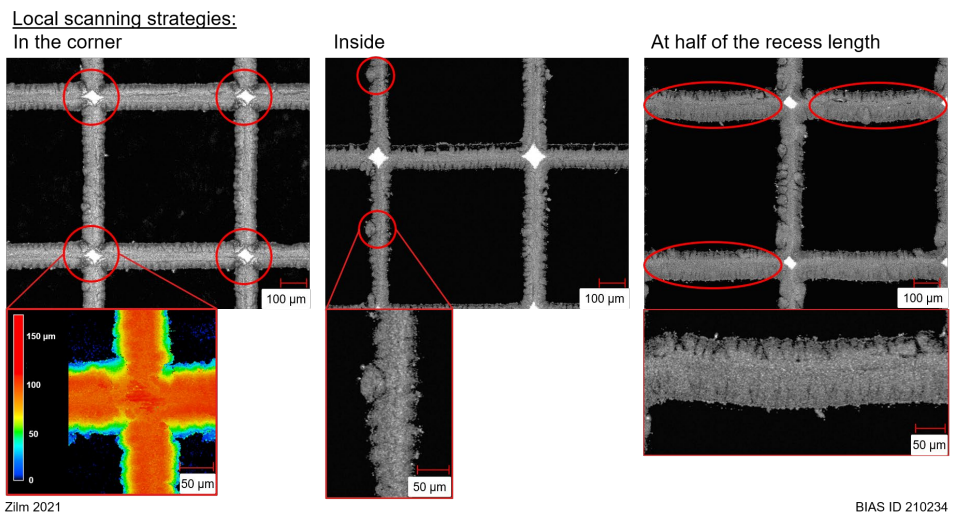

Fig. 9. Effects of laser start and end points on the bar structure

4. Discussion

The literature has shown that ridge width deviations occur when machining grids. Simons et al. and Czotscher have already shown that the ridge width deviation could be reduced to less than 8 µm by machining the cutouts helically from the inside to the outside or by machining the cutouts at a distance greater than one

cutout width from the previously machined cutout. With reference to the work of Simons et al. and Czotscher, as well as the research conducted in this study, it was confirmed that line-by-line machining results in a higher standard deviation, compare Fig. 6. The global strategy of processing the cutouts from the inside to the outside with the largest possible distance in between can significantly reduce standard deviation of the ridge width compared to line-by-line processing. In combination with the local scanning strategies "inside", standard deviations of the ridge width of 3 µm were thus achieved.

Fig. 5 shows that the global as well as the local scan strategy have to be considered together in order to reduce the difference between the measured and nominal ridge width, as well as to reduce the difference between the measured and nominal transmission, compare Fig. 8. For example, the scanning strategies "in the center of the cutout" and "inside" achieved the best possible values for the nominal ridge width, i.e., those for which the difference from the real ridge width is the smallest. The results also showed that the ridge width deviation increases for grids with narrower ridges. This seems to be due to the smaller area for heat dissipation of the ridges. As the transmission coefficient increases, the area of the ridges decreases, which can lead to heat buildup. This correlation has already been described by Czotscher 2016 for the production of grids with the nanosecond laser.

The investigations also showed that the local scanning strategy, i.e., the start and end points of the laser have a significant influence on imperfections at the ridges. Besides the described defects (cracks and not cut out slugs) and the burr formation imperfection by Simons et al, further imperfection occurred, which mainly depend on the start and end points of the laser. These imperfections are necking at the account points, local thickening and ridge deformation. According to Simons et al., the deformation originated from thermal stresses and expansions associated with low stiffness of the ridges. The deformation of the ridges was mainly observed for the local scanning strategy "in half of the indentation". In contrast, necking at the node occurred more frequently with the local scanning strategy "in the corner". The local scanning strategies "inside" resulted in thickening only at the laser turn-off point. To avoid the thickening, this scanning strategy can be optimized so that the laser endpoint is also inside.

5. Conclusion

The following conclusions can be drawn from the investigations: In order to achieve the nominal ridge width and nominal transmission, both the global and local scanning strategy must be taken into account. Thereby, the standard deviation of the ridge width can mainly be reduced by a suitable global strategy. Imperfections at the ridges i.e. necking at the account points, local thickening and ridge deformation can be reduced or even prevented by the local scanning strategy.

Acknowledgements

Funding of this work from the Deutsche Forschungsgemeinschaft (DFG) within the project “Thermischer Drift beim Laserschneiden von metallischen Netzen” under project no. 424264718 is gratefully acknowledged.

References

Baumann, R.; Lasagni, A. F.; Herwig, P.; Wetzig, A.; Leyens, C.; Beyer, E. (2019): Efficient separation of battery materials using remote laser cutting–high output performance, contour flexibility, and cutting edge quality. Journal of Laser Applications 31 (2), p 22210.

Czotscher, T.; Vollertsen, F. (2016a): Hoch transmissive metallische Sensor - komponenten hergestellt durch Laserperforieren und Umformen von Feinblechen. Laser Magazin (3), pp 13–14.

Czotscher, T.; Vollertsen, F. (2016b): Analysis of Melting and Melt Expulsion During Nanosecond Pulsed Laser Ablation. Physics Procedia 83, pp 53–61.

Czotscher, T.; Vollertsen, F. (2017): Laser processing of aluminium sheets with low heat related deformations for deep drawing. Journal for Technology of Plasticity 42 (2), pp 1–10.

Gillner, A.; Gretzki, P. (2015): Micromanufacturing engineering and technology. In: Laser Micro-structuring. 2. ed. Oxford, UK, Amsterdam: William Andrew an imprint of Elsevier; Elsevier Micro and Nano Technologies, pp 107-119.

Gladush, Gennady G. (2011): Physics of Laser Materials Processing. Theory and Experiment. Berlin, Heidelberg: Springer-Verlag Berlin Heidelberg. Springer Series in Materials Science, p 146.

Leone, C.; Genna, S.; Tagliaferri, F.; Palumbo, B.; Dix, M. (2016): Experimental investigation on laser milling of aluminium oxide using a 30W Q-switched Yb:YAG fiber laser. Optics & Laser Technology 76, pp 127–137.

Mangang, M.; Seifert, H. J.; Pfleging, W. (2016): Influence of laser pulse duration on the electrochemical performance of laser structured LiFePO4 composite electrodes. Journal of Power Sources 304, pp 24–32.

Park, D.; Lee, D. (2021): Effect of Fluence and Multi-Pass on Groove Morphology and Process Efficiency of Laser Structuring for 3D Electrodes of Lithium-Ion Batteries. Materials 14 (5).

Pfleging, W. (2018): A review of laser electrode processing for development and manufacturing of lithium-ion batteries. Nanophotonics 7 (3), pp 549–573.

Qin, Y.; Wan Nawang, W. A.; Zhao, J. (2015): Micromanufacturing engineering and technology. In: Forming of Micro-sheet Metal Components. 2. ed. Oxford, UK, Amsterdam: William Andrew an imprint of Elsevier; Elsevier Micro and Nano Technologies, pp 299-322.

Schulz, W.; Eppelt, U.; Poprawe, R. (2013): Review on laser drilling I. Fundamentals, modeling, and simulation. Journal of Laser Applications 25 (1), pp. 1-17.

Simons, M.; Rusche, T.; Valentino, T.; Radel, T.; Vollertsen, F. (2020): UKP-laserbasierte Herstellung von Netzen unterschiedlicher Transmissionsgrade/USP-laser based production of meshes of different transmission degrees. wt 110 (11-12), pp 787–789.

Tóth, L.; Goto, K. M., Hiroyuki, M.; Fumihiko, M.; Hiroshi, D. (2011): New 1π sr acceptance angle display-type ellipsoidal mesh analyzer for electron energy and two-dimensional angular distribution as well as imaging analysis. Nuclear Instruments and Methods in Physics Research Section A: Accelerators, Spectrometers, Detectors and Associated Equipment 648, pp 58-59.